

AT2021acak: a candidate tidal disruption event found in the Zwicky Transient Facility survey

Jie Li¹, Zhong-Xiang Wang^{1,2,3}, Dong Zheng¹, Ju-Jia Zhang^{4,5,6}, Li-Tao Zhu¹ and Zhang-Yi Chen¹

¹ Department of Astronomy, School of Physics and Astronomy, Yunnan University, Kunming 650091, China; wangzx20@ynu.edu.cn

² Shanghai Astronomical Observatory, Chinese Academy of Sciences, 80 Nandan Road, Shanghai 200030, China

³ Purple Mountain Observatory, Chinese Academy of Sciences, Nanjing 210034, China

⁴ Yunnan Observatories, Chinese Academy of Sciences, Kunming 650216, China

⁵ Key Laboratory for the Structure and Evolution of Celestial Objects, Chinese Academy of Sciences, Kunming 650216, China

⁶ Center for Astronomical Mega-Science, Chinese Academy of Sciences, 20A Datun Road, Chaoyang District, Beijing 100012, China

Received 20xx month day; accepted 20xx month day

Abstract We report a candidate tidal disruption event (TDE) found in the Zwicky Transient Facility (ZTF) survey data. This candidate, with its transient name AT2021acak, showed brightness increases of ~ 1 mag around MJD 59500 and subsequent power-law-like brightness declines. We have conducted multiple optical spectroscopic observations with the 2.4-m Lijiang telescope and one observation at X-ray and ultraviolet (UV) bands with the *Neil Gehrels Swift Observatory* (*Swift*). The optical spectra of the source show broad H and He emission line and Fe emission features. Possible 0.3–2 keV X-ray and bright UV emission of the source was detected. We analyze the declines of the optical light curves, the emission features of the optical spectra, and the constructed broad-band UV and optical spectrum. The properties derived from the analyses are consistent with those of reported (candidate) TDEs, and in particular very similar to those of ASASSN-18jd. The identification is complicated by the host being likely an AGN, and thus further observations of the event and quiescent host are required in order to have a clear understanding of the nature of this transient event.

Key words: transients: tidal disruption events — galaxies: nuclei — quasars: emission

1 INTRODUCTION

When a star moves too closely to the central massive black hole (MBH) of a galaxy, for example ~ 1 AU for a solar-mass star to a $10^7 M_\odot$ MBH, it will be under tidal forces exerted by the MBH that are stronger than its own gravitational force, and thus be disrupted. Approximately half of the star’s mass will be bounded by the gravitational potential of and subsequently accreted by the MBH. During this so-called tidal disruption event (TDE), the accretion will power transient radiation from the MBH that is otherwise often in a non-active state. While the TDEs have been long proposed and widely explored theoretically (e.g., Hills 1975; Rees 1988; Evans & Kochanek 1989; Strubbe & Quataert 2009; Lodato & Rossi 2011; Guillochon et al. 2014; Kochanek 2016; Dai et al. 2018; Mockler et al. 2019; Coughlin & Nixon 2019), more and more observational discoveries of them have been reported in recent years (e.g., van Velzen et al. 2021b; Gezari 2021) enabled by the fast-growing capability of the transient surveys. Studies of TDEs can probe properties of dormant MBHs in galaxies, transient accretion processes, and stellar dynamics close to the center of galaxies (see Gezari 2021 and references therein).

Main observational discoveries of TDEs started with the ROSAT all-sky survey at X-rays (Donley et al. 2002), and continued with the transient surveys at optical wavelengths such as the Palomar Transient Factory (e.g., Arcavi et al. 2014) and All-Sky Automated Survey for Supernovae (e.g., Holoien et al. 2014). As the

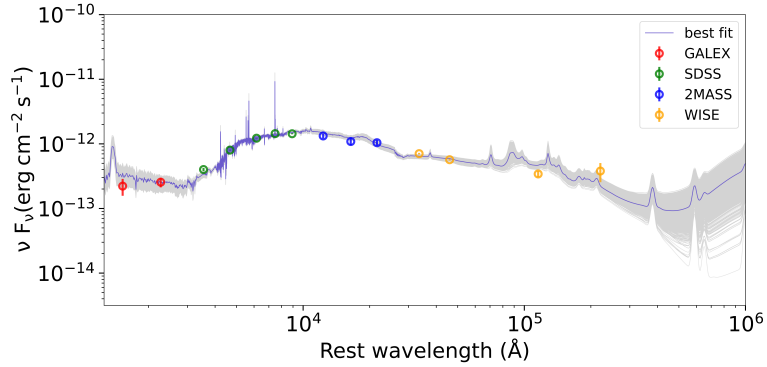


Fig. 1: Broad-band SED of J1034+1529 in its presumably quiescent state. It can be fit with AGN type spectra, which are indicated by the gray line region and were generated from the code PROSPECTOR.

Zwicky Transient Facility (ZTF; Bellm et al. 2019) represents the latest, more powerful optical surveys, with respect to its large field of view (47 deg^2) and high cadence ($\sim 2 \text{ day}$), it can serve as a powerful facility for finding TDEs (and other similar transient events). Indeed, van Velzen et al. (2021b) reported 17 new TDEs recently detected in the ZTF survey. These TDEs, plus the previously reported ones, show a variety of features that not only reveal the accretion-related physical processes but also present different challenges to theoretical studies, thus helping improve our full understanding of the TDE phenomenon (Gezari 2021).

As we have been exploring the ZTF data, one source (named AT2021acak in the transient name server¹) was found to have the light curves resembling those of the TDEs. Simultaneous infrared brightening of the source was also found in the NEOWISE Post-Cryo survey data obtained with the Wide-field Infrared Survey (WISE; Wright et al. 2010). We thus arranged optical spectroscopic observations with the 2.4-m Lijiang telescope and a Target of Opportunity (ToO) observation at X-ray and ultraviolet (UV) bands with the *Neil Gehrels Swift Observatory* (*Swift*) (Gehrels et al. 2004). In this paper, we report the results from the observations for this transient event case.

AT2021acak arises from a source with a position of R.A. = $10^{\text{h}}34^{\text{m}}47^{\text{s}}.99$, Decl. = $+15^{\circ}29'22''.42$ (J2000.0). Hereafter we use name J1034 for this source. As there are previous observational data for the source obtained from different surveys, we first collected the information and studied its likely source type. A brief description of the data and our source-type analysis is presented in Section 1.1. We then describe the data that were taken during the time period just before and over the transient event of the source. The data include those from the ZTF and WISE surveys and our observations as well. The data description and reduction processes are given in Section 2. The related analyses and results are presented in Section 3. We discuss the results in Section 4, which points out this transient case as a candidate TDE. In this work we used the latest cosmological parameters determined from the Planck mission (Planck Collaboration et al. 2020), $H_0 \simeq 67.4 \text{ km s}^{-1} \text{ Mpc}^{-1}$ and $\Omega_m = 0.315$.

1.1 Source J1034+1529

The source J1034 has been detected in different surveys, which include the Galaxy Evolution Explorer (GALEX; Bianchi et al. 2011), the Sloan Digital Sky Survey (SDSS; Adelman-McCarthy & et al. 2009), the Two Micron All Sky Survey (2MASS; Cutri et al. 2003), and the WISE (Cutri & et al. 2012). Its infrared colors were $J - K_s = 1.31$ and $K_s - W3 = 4.01$ or mid-infrared (MIR) colors were $W1 - W2 = 0.78$ and $W2 - W3 = 2.19$. The both suggest a quasar (e.g., Wright et al. 2010; Tu & Wang 2013). Indeed, J1034 is included as a quasar in the Million Quasar catalog (version 7.2; Flesch 2021).

We constructed its broad-band spectral energy distribution (SED; see Figure 1) based the flux measurements mentioned above, which were approximately obtained before 2012. While the measurements were not simultaneous and the SED might not be a true ‘quiescent’ one, we used the code PROSPECTOR (Johnson et al. 2021) to fit the SED. The result is shown in Figure 1, for which the parameter $f_{\text{agn}} \simeq 0.27$ (see Leja et al. 2018 for details). This parameter value suggests a significant AGN contribution in the emission of J1034.

¹ <https://www.wis-tns.org/object/2021acak>

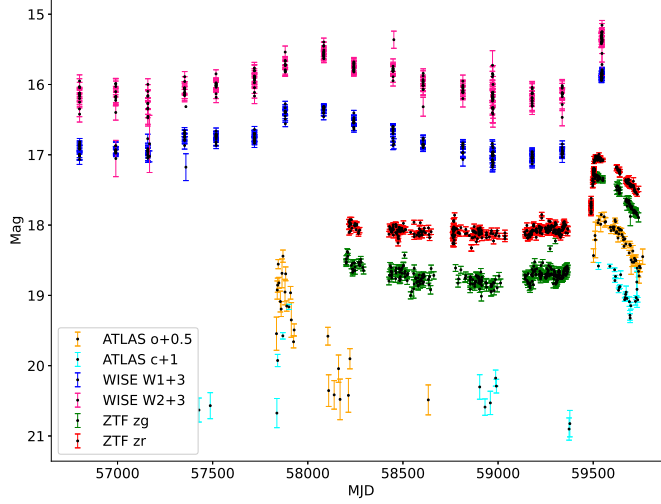


Fig. 2: Optical and MIR light curves of J1034+1529, the latter of which are down-shifted by 3 mag to be shown in one panel. The ATLAS light curves, which were constructed by excluding data points with either magnitudes ≥ 20 (Tonry et al. 2018) or uncertainties > 0.3 mag, show a flare-like event around MJD 57800. Around MJD 59500, there is a brightness jump seen in the both ATLAS and ZTF optical and WISE MIR bands.

We note that the source also showed flux variations at optical bands. Revealed by the optical light curves obtained with the Asteroid Terrestrial-impact Last Alert System (ATLAS; Tonry et al. 2018), a ~ 100 d flare-like event around MJD 57800 is seen (Figure 2). The event lasted relatively short and then the source went back to its previous quiescent magnitude level. Thus this variation event likely is another piece of evidence, in addition to the above, that points to an AGN for J1034.

2 DATA AND OBSERVATIONS

2.1 Light Curve data

As we explored the ZTF light curve data with the Automatic Learning for the Rapid Classification of Events (ALeRCE; Förster et al. 2021; Sánchez-Sáez et al. 2021), we noted this source’s recent flaring-like activity starting from \sim MJD 59500: after the sudden brightening, the light curves have been going through a power-law decline. We downloaded the *zg* and *zr* band light curve data from the ZTF public Data Release 11 (released on 2022 May 9). For keeping the cleanliness and goodness of the data, we required *catflags*=0 and *chi* < 4 when querying the ZTF data. Also in order to have as many data as possible, we included those data points available through ALeRCE². The *zg* and *zr* light curves are shown in Figure 2. The ATLAS light curves show a similar pattern. However because their bands are not regular ones and the limiting magnitudes are only slightly larger than 19 (Tonry et al. 2018), the latter resulting in only a few data points before the brightening, we did not include the ATLAS light curves in the further analysis.

We also checked the source’s MIR W1 ($3.4 \mu\text{m}$) and W2 ($4.6 \mu\text{m}$) light curve data, and downloaded them from the WISE NEOWISE-R Single-exposure Source database. In Figure 2, the MIR light curves are shown. As can be seen, a related brightening also occurred at the MIR wavelengths, although the data were basically from one-epoch of observations. The average magnitudes (in MJD 59000–59500) of the source before the brightening are W1=14.00 and W2=13.17, and at the brightening (average time MJD 59545) are W1=12.87 and W2=12.35. Therefore the source brightened by 1.1 and 0.8 mag at W1 and W2 bands respectively.

² <https://alerce.online/>

Table 1: Information for spectroscopic observations of J1034

Date (UT)	Grism	Slit width ($''$)	Seeing ($''$)	Exposure (s)
2022-04-23	G15	5.0	1.8	900
2022-04-23	G15	5.0	1.8	900
2022-04-24	G3	2.5	2.1	900
2022-04-25	G3	2.5	2.1	1200
2022-06-03	G3	2.5	1.7	1350

2.2 Spectroscopic observations

Five spectroscopic observations of J1034 were conducted with the 2.4-m Lijiang telescope. The instrument used was YFOSC (Wang et al. 2019). Its detector is a 2048×4608 pixel² back-illuminated CCD and the pixel scale is $0.283''$ pixel⁻¹. In the observations, a G15 (or G3) grism was chosen, providing the wavelength coverage of 4100–9800 Å (or 3400–9100 Å) and the spectral dispersion of 3.9 Å pixel^{-1} (or 2.9 Å pixel^{-1}). A long slit was used, and its width was set to be either $5.0''$ or $2.5''$ (see Table 1). In each observation, we also took the spectrum of a He-Ne lamp for wavelength calibration and that of the spectrophotometric standard BD+33d2642 for flux calibration, while with the same instrument setup as that for the target. The information for the observations, including the exposure times, are summarized in Table 1.

The spectrum images were routinely processed using the IRAF tasks, which included bias-subtraction and flat-fielding. Spectrum extraction and calibration were conducted using the standard routines in IRAF as well.

2.3 *Swift* Observation

We requested a ToO observation of the source with *Swift*. The observation (obsid 00015141001) was conducted on 2022 April 28. The photon counting mode and image mode were respectively used in the X-ray Telescope (XRT) and the Ultraviolet/Optical Telescope (UVOT) exposures. The lengths of the exposures were approximately 1500-s long, and the filter UVW2 (central wavelength 1928 Å; Poole et al. 2008) was used in the UVOT exposure.

We used the online tools³ for the XRT data analysis and source detection (Evans et al. 2020). No detection of the source was found, while we tested different energy bands such as 0.3–1 keV, 1–2 keV, and 2–10 keV. However when we used the light curve tool (Evans et al. 2007, 2009), a count rate of $(4.6 \pm 2.1) \times 10^{-3} \text{ cts s}^{-1}$ in 0.3–2 keV was derived, which was indicated to be higher than that of the background by a 3σ confidence level. We checked the individual photons but could not determine if this marginal detection was real or not. We considered this count rate as an upper limit (but discuss the detection possibility in Section 4). In 2–10 keV, an upper limit of $5.3 \times 10^{-3} \text{ cts s}^{-1}$ (3σ) was obtained.

In order to convert the count rate to flux, we used the tool PIMMS. We tested blackbody and power-law models, where the Galactic hydrogen column density $3.1 \times 10^{20} \text{ cm}^{-2}$ (HI4PI Collaboration et al. 2016) was assumed. The resulting unabsorbed flux upper limits in 0.3–2 keV were in a range of $1.1\text{--}1.6 \times 10^{-13} \text{ erg cm}^{-2} \text{ s}^{-1}$, depending on the model assumed. We adopted the middle value, $1.4 \times 10^{-13} \text{ erg cm}^{-2} \text{ s}^{-1}$, as the flux upper limit for the source.

The source was detected in the UVOT exposure. We ran the tool `uvotsource` and obtained a magnitude of 16.71 ± 0.05 for the source, where a circular source region with radius $5''$ and a circular background region with radius $15''$ were used. The magnitude corresponds to a flux of $2.14 \pm 0.10 \times 10^{-12} \text{ erg cm}^{-2} \text{ s}^{-1}$.

3 RESULTS

3.1 Optical light curves

The detailed optical light curves before (in quiescence) and covering the flare event are shown in the left panel of Figure 3. The average fluxes in quiescence (shown in Figure 3) are 0.118 ± 0.012 and $0.213 \pm 0.014 \text{ mJy}$ in *zg* and *zr* band respectively, where the uncertainties were estimated as the standard deviations of each quiescent light-curve part. We studied the light curves by fitting them with a model typically considered for TDEs. The model (e.g., van Velzen et al. 2021b) is given as 1) $F(t) =$

³ https://www.swift.ac.uk/user_objects/

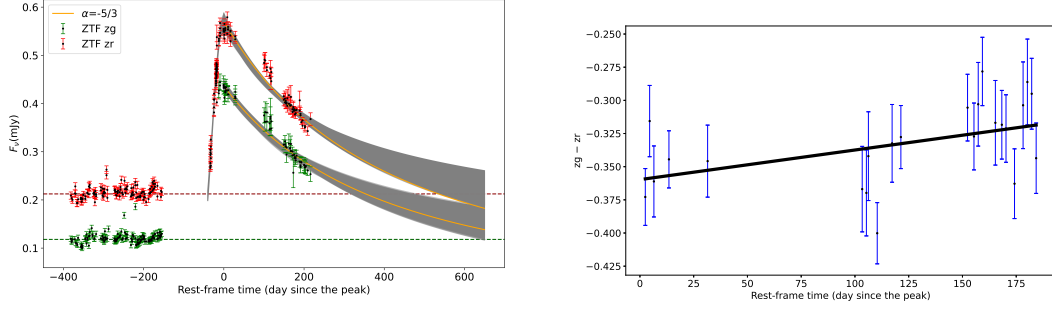


Fig. 3: *Left panel*: Optical light curve fitting with a typical TDE model (gray regions). The flux density declines since the peak as a function of time $t^{-5/3}$ are marked with orange curves. The average fluxes at zg and zr bands before the flare are marked with the dashed lines. *Right panel*: $zg - zr$ colors during the flare, for which a rate of $2.2 \pm 0.8 \times 10^{-4} \text{ day}^{-1}$ (black line) is derived.

$F_p \exp[-(t - t_p)^2 / 2\sigma_t^2]$ when $t \leq t_p$, and 2) $F(t) = F_p[(t - t_p + t_0)/t_0]^\alpha$ when $t \geq t_p$, where t is time and the flux $F(t)$ has a peak F_p at time t_p . In this model, the first function is a Gauss with standard deviation σ_t and the second is a power law with index α and normalization t_0 .

We used the Markov Chain Monte Carlo (MCMC) code `emcee` (Foreman-Mackey et al. 2013) for the fitting, in which the times of the data points were shifted to the rest frame with $z = 0.136$ (see Section 3.2). As the flux rise of the event was caught in zr band, this part was fitted with the Gaussian function and t_p and σ_t were determined to be MJD 59522 and 27 day. The event would have started from MJD 59489. The peak fluxes were 0.44 and 0.58 mJy in zg and zr band respectively. We then fixed $t_p = 59522$ and fit the decline parts of the light curves with the power-law function. The function can approximately describe the light curves, but a few data points in the middle appear to deviate away from a power law (Figure 3). The index ranges (1σ) found from the fitting were $(-2.08, -0.64)$ for the zg band and $(-1.26, -0.61)$ for the zr band. Both the ranges are large, probably due to the sparseness of the data points, and the second one is flatter than the typical $-5/3$ decline (Coughlin & Nixon 2019). We suspect that there could be a break in the decline parts; for example in zg band, the light curve could be considered to be relatively flat from the peak to the middle (with $\alpha \sim -0.6$) and turn steep in the latter part (with $\alpha \sim -1.2$).

Since colors and color changes can be used as a parameter to discriminate TDE from other types of transients/variations (van Velzen et al. 2021b), we calculated the $zg - zr$ values during the flare time (right panel of Figure 3). The two-band magnitudes obtained in the same night were considered to be simultaneous and used in the calculation. Over ~ 200 days, the observed $zg - zr \sim 0.3$, but we should take into account the color in quiescence especially when the magnitude changes caused by the flare were not very large. As J1034 had the average $zg - zr \simeq 0.636 \pm 0.005$ in quiescence, $zg - zr$ values (~ -0.34) shown in the right panel of Figure 3 were calculated by subtracting the quiescent color value from the observed ones (similar information also presented in Section 3.3). Only a small rate of $2.2 \pm 0.8 \times 10^{-4} \text{ day}^{-1}$ for the color values during the flare was derived. Thus the blue color during the flare and its close-to-zero rate are consistent with those of TDEs (van Velzen et al. 2021b).

3.2 Features of the optical spectra

The obtained spectra are shown in Figure 4. Broad hydrogen Balmer ($H\alpha$ – $H\delta$) and helium ($\text{He II } \lambda 4686$ and $\text{He I } \lambda 5875$) emission lines were detected. It can be noted that $H\alpha$ on April 24 (the third one in Table 1) appears as the strongest. In addition, there are Fe II emission (e.g., Blanchard et al. 2017; He et al. 2021) visible, particularly in the 5000–5500 Å region (see also Figure 5), and weak but notable $[\text{Fe XIV}] \lambda 5304$ and $[\text{Fe X}] \lambda 6376$ emission lines (e.g., Wang et al. 2012).

In order to study the properties of these emission features, we used the Python QSO fitting code (PyQSOFit; Guo et al. 2018). As shown in Section 1.1, J1034 is likely an AGN when in its quiescent state. Also in our fitting, we could only find a weak (or rather uncertain) galaxy component. Thus the code likely provided sufficiently good results for the properties of the emission features. The main regions studied were those around the $H\alpha$ and $H\beta$ respectively, and the Fe II emission from 3686 Å to 7484 Å (Boroson & Green 1992) was considered as well.

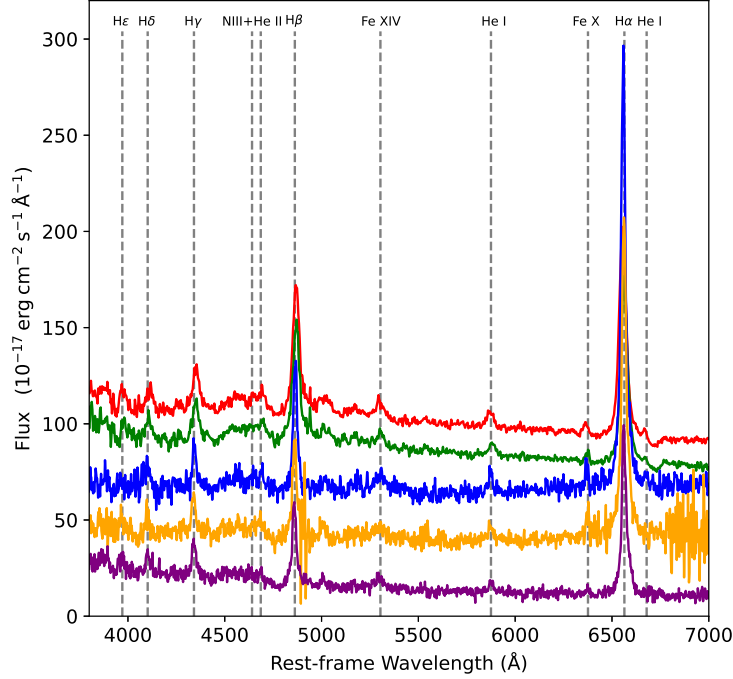


Fig. 4: Optical spectra of J1034, which follow the sequence given in Table 1 from the above to bottom. For clarity, they are slightly shifted in the vertical direction. A few emission lines detected in the spectra are marked, which include Balmer lines, He I $\lambda 5875$, and He II $\lambda 4686$. Also weak [Fe XIV] $\lambda 5304$ and [Fe X] $\lambda 6376$ are seen.

Since we found that a single Gaussian function could not well fit the two prominent Balmer lines, we added a narrow component. An example of the spectral fitting is shown in Figure 5. In addition, the line He II $\lambda 4686$ was fitted in the same way, as a broad component was needed in the fitting. The lines [Fe XIV] $\lambda 5304$ and [Fe X] $\lambda 6376$ were fitted with one component, although for the last two of our spectra, [Fe X] could not be determined. The measurement results for the five spectra are given in Table 2. The uncertainties of the line measurements were derived from a MCMC method recently included in the code, and for the Fe II emission, we followed the method in He et al. (2021) and the uncertainties were estimated as the standard deviations of the results from fitting 100 times. Based on the measurements for the narrow components, redshift $z = 0.136$ was determined.

In the fitting, we suspect that the two components, a broad plus a narrow one, may not be able to correctly derive the strengths of each of them, although they can well describe the total line profiles. For example, there is not a clear trend for the changes of the line components, and the brightest H α (on April 24) was caused by the enhancement of the narrow component. There were also the cases that an additional broad continuum-like component was needed in the fitting (e.g., the H β region shown in the left-middle panel of Figure 5). In any case, the FWHMs of the narrow components of the lines are generally consistent with each other, as the values are in a range of 800–1100 km s $^{-1}$. The FWHMs of the broad components of H α and H β can also be noted to mostly be ~ 3000 km s $^{-1}$. In addition, the Fe II emission is shown to be roughly declining from the first to the last.

The presence of the line He II $\lambda 4686$, as well as N III $\lambda 4640$, was required; otherwise the fitting would end with a residual bump at the position and a larger χ^2 value (see Figure 5). However the broad component in the fitting was highly uncertain, probably due to low signal-to-noise ratios of the detections and the mixture with the Fe II emission. We carefully examined the the region and for the spectrum 2–5, the component was more likely added so that the resulting χ^2 could be minimized. We thus only report the results for spectrum 1, for which the fitting is shown in Figure 5.

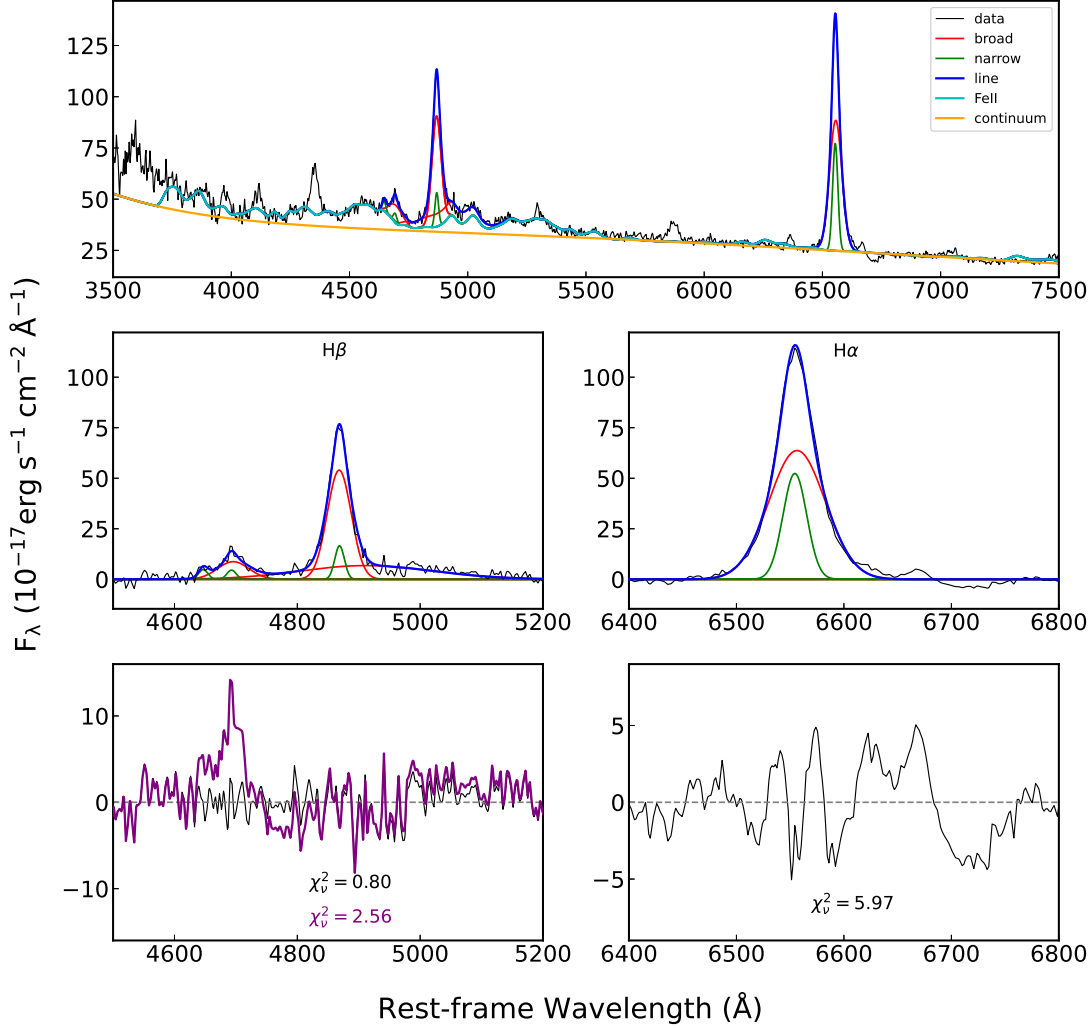


Fig. 5: Example of the fitting to the optical spectra of J1034, where the first one (in Table 1) is shown. The fitting included the Fe II emission (3686–7484 Å; top panel). Two main regions covering H α and H β are shown in the middle and bottom panels (line fitting and residuals, respectively). One broad (red line) and one narrow (green line) component are needed to fit the prominent H α and H β lines. In the H β region, the existence of the lines He II λ 4686 and N III λ 4640 is needed; otherwise a residual bump at their position would appear and induce larger χ^2 in the fitting.

3.3 Broad-band spectrum

Provided with the X-ray flux upper limit and UV flux obtained in the *Swift* observation, we constructed the broad-band spectrum of the source in the flaring state on 2022 April 28. The ZTF measurements on the date were 17.730 ± 0.031 and 17.427 ± 0.025 mag in zg and zr band respectively. The average quiescent optical fluxes in the two bands were subtracted from them. For the UV flux, we estimated a quiescent value by linear interpolation from the two GALEX data points and the value was subtracted as well. As the Galactic extinction towards the source is $E(B-V) \simeq 0.032$ (Schlafly & Finkbeiner 2011), we used this value and the extinction law given by Cardelli et al. (1989) to deredden the UV and optical fluxes. Then the wavelengths of the X-ray, UV, and optical were shifted back to the rest frame with $z = 0.136$. The resulting spectrum is shown in Figure 6.

Since emission of TDEs has a thermal origin (Gezari 2021), we estimated the properties of the blackbody emission of the flare event by fitting the broad-band spectrum. Because there are only three data points, no effort was made to search for a complete range of blackbody parameters that can provide fits to the data

Table 2: Measurements for the emission features

Line	2022-04-23 (First)	2022-04-23 (Second)	2022-04-24	2022-04-25	2022-06-03
H α broad					
FWHM	2427.1 \pm 41.8	2501.1 \pm 16.6	2891.6 \pm 60.7	3048.4 \pm 97.1	2696.1 \pm 59.5
EW	199.7 \pm 10.6	201.5 \pm 3.2	185.9 \pm 10.5	195.1 \pm 16.3	184.5 \pm 10.2
Flux	4956.6 \pm 262.1	4182.1 \pm 67.3	5305.1 \pm 300.6	4256.3 \pm 357.1	2439.0 \pm 134.9
H α narrow					
FWHM	850.2 \pm 28.5	845.9 \pm 1.5	848.7 \pm 15.3	848.7 \pm 7.8	825.5 \pm 17.5
EW	22.3 \pm 3.3	31.1 \pm 1.0	113.7 \pm 4.5	111.5 \pm 4.6	100.4 \pm 4.6
Flux	552.9 \pm 80.7	645.9 \pm 21.7	3242.9 \pm 128.4	2431.2 \pm 100.4	1328.6 \pm 61.4
H β broad					
FWHM	2831.9 \pm 18.0	2882.3 \pm 48.9	2881.3 \pm 79.5	2860.2 \pm 75.9	3308.4 \pm 157.7
EW	76.8 \pm 1.6	77.2 \pm 2.9	55.8 \pm 5.0	57.9 \pm 5.8	59.6 \pm 7.7
Flux	2641.9 \pm 56.7	2330.1 \pm 88.7	1367.7 \pm 123.1	1156.7 \pm 117.4	1057.6 \pm 138.2
H β narrow					
FWHM	1123.8 \pm 12.6	1122.6 \pm 14.4	1116.1 \pm 20.3	1085.4 \pm 46.3	1096.3 \pm 44.9
EW	9.3 \pm 0.5	11.2 \pm 0.9	37.8 \pm 2.4	32.6 \pm 3.7	38.9 \pm 3.2
Flux	320.6 \pm 17.8	338.6 \pm 28.8	926.6 \pm 60.5	650.4 \pm 74.4	691.1 \pm 58.1
HeII broad					
FWHM	3648.0 \pm 90.0	-	-	-	-
EW	15.0 \pm 0.7	-	-	-	-
Flux	530.5 \pm 24.9	-	-	-	-
HeII narrow					
FWHM	1123.8 \pm 12.6	1122.6 \pm 14.4	1116.1 \pm 20.3	1085.4 \pm 46.3	1096.3 \pm 44.9
EW	2.3 \pm 0.1	3.4 \pm 0.2	2.8 \pm 1.9	2.9 \pm 0.7	6.1 \pm 1.0
Flux	80.5 \pm 3.4	106.02 \pm 7.7	57.3 \pm 52.9	59.9 \pm 16.1	117.9 \pm 19.3
Fe X					
FWHM	1047.2 \pm 78.1	842.3 \pm 87.9	788.6 \pm 94.5	823.1 \pm 73.7	978.1 \pm 168.4
EW	4.7 \pm 0.7	3.9 \pm 0.7	9.0 \pm 2.1	12.9 \pm 2.2	5.9 \pm 2.1
Flux	124.1 \pm 17.9	84.5 \pm 16.7	249.4 \pm 58.5	271.0 \pm 48.0	78.9 \pm 27.3
Fe XIV					
FWHM	1019.8 \pm 120.9	1108.3 \pm 86.8	951.3 \pm 208.1	-	-
EW	3.9 \pm 0.8	4.0 \pm 0.7	5.6 \pm 2.1	-	-
Flux	124.4 \pm 26.4	111.0 \pm 19.8	137.6 \pm 52.1	-	-
Fe II emission					
Flux	12224.7 \pm 3373.8	10554.7 \pm 228.9	11231.8 \pm 3558.6	8960.9 \pm 22.7	8090 \pm 86.6

Notes: Full width at Half Maximum (FWHM), equivalent Width (EW), and flux measurements are in units of km s^{-1} , angstrom (\AA), and $10^{-17} \text{ erg cm}^{-2} \text{ s}^{-1}$, respectively.

points. Instead, we tested different temperature values and searched for the best fits around the values. We found a likely good fit when the blackbody temperature is 1.48 eV (or 17160 K) and the spherical radius is $2.9 \times 10^{-4} \text{ pc}$ (or $8.9 \times 10^{14} \text{ cm}$ for a source distance of 665 Mpc). The reduced χ^2 is large, $\chi^2 \simeq 15$. This large χ^2 value probably reflects that the spectral data points would have larger uncertainties; for example, the quiescent UV flux was estimated from the measurements obtained long time ago and the times of the data points were only on the same date but not exactly simultaneous.

4 DISCUSSION

Exploring the ZTF data, we have found a TDE-like optical flaring event. We have requested follow-up observations and conducted multi-wavelength studies of the event source. By studying the ZTF light curves, we have found that the flare can be described with a typical TDE model, a Gaussian rise plus a power-law decline. While the light curve data and power-law index do not follow the exact $\alpha = -5/3$ decline, there have been many cases showing variations from the typical decline (e.g., van Velzen et al. 2021b) and the physical reasons for the variations have been discussed (e.g., Lodato & Rossi 2011; Coughlin & Nixon 2019). From the fitting, we have estimated that the event started from MJD 59489 (or -33 days from t_p) and would last for more than 500 days. In addition, the optical color $zg - zr$ and its changes during the flare were found to be ~ -0.34 and close to zero respectively. These values are typical for TDEs (e.g., van Velzen et al. 2021b).

We have also found MIR brightening from the WISE light curve data. The flux increments were 1.4 and 1.1 mJy in W1 and W2 band respectively. The corresponding luminosity of the flare at W1 band was $\nu L_\nu \simeq 7.4 \times 10^{43} \text{ erg s}^{-1}$. This value is substantially higher than those derived for TDEs found in non-active galaxies (Jiang et al. 2021) but in the range for the TDEs in AGN (van Velzen et al. 2021a). The luminosity

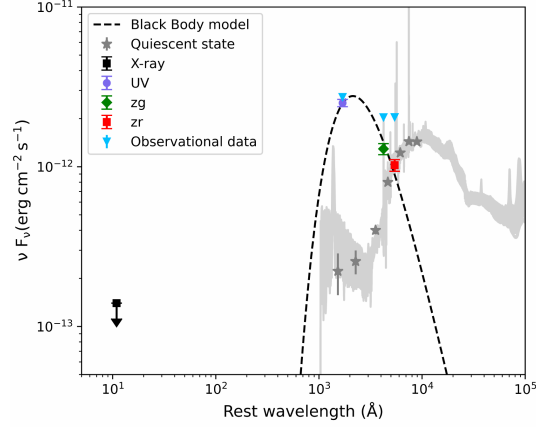


Fig. 6: Optical and UV fluxes and X-ray flux upper limit of J1034 on 2022 April 28 (MJD 59697). The quiescent SED in Figure 1 is plotted to show the flux changes. After being subtracted with the corresponding quiescent fluxes, the optical and UV data points can approximately be fitted with a blackbody of temperature 1.48 eV and spherical radius 2.9×10^{-4} pc (dashed curve).

difference has been discussed to reflect the available dust covering the central MBHs; AGN contain a dust torus such that they are seen to show more luminous MIR emission when TDEs occur (Jiang et al. 2021). The high MIR luminosity thus supports J1034 as an AGN when the source is in quiescence. The average time for the brightening is MJD 59545, which is larger than t_p in our optical light curve fitting by 23 days. Because we do not know the exact peak time in the MIR data due to the large observational gaps of the data and the MIR brightening in TDEs usually has a delay time, i.e., the MIR peak time with respect to t_p , in a range of ~ 100 – 200 days (van Velzen et al. 2021a), we may consider that the delay time τ would be $\tau \geq 23$ day. This delay time can be used to estimate the distance of the dust to the MBH in this system, which would be $\sim c\tau/(1+z) \geq 0.02$ pc (where c is the speed of light).

The optical spectra contain H and He emission lines, which would suggest that this candidate TDE belongs to the H+He class. However given the host likely being an AGN, the emission features or some of them could be intrinsic ones. We note that our spectra are very similar to those reported for ASASSN-18jd (Neustadt et al. 2020). The both have FWHMs ~ 3000 km s $^{-1}$ broad H α and H β lines, weak He II $\lambda 4684$ and N III $\lambda 4640$ lines that are overlapped with the Fe II emission, and weak coronal lines [Fe XI] and [Fe X]. Neustadt et al. (2020) have extensively discussed the features and their variations over the flare event, and concluded that ASASSN-18jd could be a TDE or a new type of transient driven by the MBH. In any case, spectroscopy of J1034 in quiescence would help clarify the nature of AT2021acak. We note that in the TDE scenario, the Fe II emission is considered as the result of sublimation of dust (e.g., He et al. 2021) by strong radiation of the TDE and the coronal lines as the result of photoionization of gas (e.g., Wang et al. 2012; Gezari 2021).

Using the UV flux measurement provided by the *Swift* observation, we have estimated a blackbody temperature of ~ 1.48 eV and a radius of $\sim 8.9 \times 10^{14}$ cm. This blackbody has negligible emission at X-rays (Figure 6), which made us not consider the marginal detection in 0.3–2 keV with *Swift*/XRT. However we note that ASASSN-18jd had X-ray emission whose luminosities were approximately an order of magnitude lower than those of its UV/optical blackbody (see Figures 3 & 5 in Neustadt et al. 2020), and the X-ray emission contained a soft, ~ 0.1 keV blackbody component. Examining our broad-band spectrum in Figure 6, the X-ray flux (shown as an upper limit), when we consider the marginal detection, would appear to be similar to that of ASASSN-18jd (i.e., the X-ray flux is an order of magnitude lower than that of the 1.48 eV blackbody). Thus there could be soft X-ray emission from J1034 just like in ASASSN-18jd and the similarity between the two cases would be further established.

The luminosity of the UV/optical blackbody for J1034 can be estimated to be 4.9×10^{43} erg s $^{-1}$. The temperature and luminosity put this source right into the group of optically selected TDEs (see Figure 2 in Gezari 2021). As a case with radius $< 10^{15}$ cm would generally indicate a H+He class TDE Gezari 2021, the radius of the blackbody in this respect is also consistent by showing both H plus He emission lines in the flare event of J1034. However we note that the blackbody luminosity is comparable to the MIR value, which suggests that the blackbody emission would have dropped significantly from the peak to 2022 April

28 (MJD 59697) over ~ 175 days. Considering the ratios of the peak luminosities at the MIR to those of the blackbody derived for TDEs (Jiang et al. 2021; Wang et al. 2022), the peak blackbody luminosity of this flare would have been at least 10 times that of the MIR, which is $\sim 10^{45} \text{ erg s}^{-1}$ and would imply that the blackbody temperature (assuming a fixed radius) had a factor of 2 decline over the course. Even assuming such a decline, the estimated peak temperature and luminosity would still put this case into the same TDE group (Gezari 2021).

As a summary, the transient AT2021acak has been found to have the following properties: 1) optical light curves can be described with a Gaussian rise plus a power-law decay while with color $zg - zr \sim -0.34$ and close-to-zero color changes during the decay; 2) optical spectra show emission features that include the prominent Balmer lines, weak helium and coronal Fe lines, and Fe II emission; 3) UV and optical emission can be described with a $\sim 1.48 \text{ eV}$ blackbody with a spherical radius of $\sim 8.9 \times 10^{14} \text{ cm}$. These properties can be indicative evidence of an H+He class TDE, while the limited observational data we have and a likely AGN host complicate the identification. However as discussed in detail by Neustadt et al. (2020) about the features of ASASSN-18jd, the similarity of AT2021acak to it would suggest a now-so-called ambiguous nuclear transient (ANT; see, e.g., Trakhtenbrot et al. 2019; Hinkle 2022) as another possibility. The number of these ANTs identified is rapidly increasing (Hinkle 2022), and their nature remains to be understood. In any case, further observations of the event are warranted as the property changes in the decline process would be obtained. Moreover, when the source goes back to its quiescent state, optical spectroscopy will be required so that we would have a better understanding of this transient event by obtaining properties of the host galaxy.

Acknowledgements This work was based on observations obtained with the Samuel Oschin Telescope 48-inch and the 60-inch Telescope at the Palomar Observatory as part of the Zwicky Transient Facility project. ZTF is supported by the National Science Foundation under Grant No. AST-2034437 and a collaboration including Caltech, IPAC, the Weizmann Institute for Science, the Oskar Klein Center at Stockholm University, the University of Maryland, Deutsches Elektronen-Synchrotron and Humboldt University, the TANGO Consortium of Taiwan, the University of Wisconsin at Milwaukee, Trinity College Dublin, Lawrence Livermore National Laboratories, and IN2P3, France. Operations are conducted by COO, IPAC, and UW. This work made use of data products from the Wide-field Infrared Survey Explorer, which is a joint project of the University of California, Los Angeles, and the Jet Propulsion Laboratory/California Institute of Technology, funded by the National Aeronautics and Space Administration.

We are grateful to *the Neil Gehrels Swift Observatory* for approving the requested ToO observation. We acknowledge the support of the staff of the Lijiang 2.4-m telescope (LJT). Funding for the LJT has been provided by the CAS and the People’s Government of Yunnan Province. The LJT is jointly operated and administrated by YNAO and the Center for Astronomical Mega-Science, CAS.

We thank the anonymous referee for very helpful and detailed comments, based on which this manuscript has been greatly improved. This research is supported by the National SKA program of China (No. 2022SKA0130101), Basic Research Program of Yunnan Province (No. 202201AS070005), and the National Natural Science Foundation of China (12273033). Z.W. acknowledges the support by the Original Innovation Program of the Chinese Academy of Sciences (E085021002).

References

- Adelman-McCarthy, J. K., & et al. 2009, *VizieR Online Data Catalog*, II/294 2
- Arcavi, I., Gal-Yam, A., Sullivan, M., et al. 2014, *ApJ*, 793, 38 1
- Bellm, E. C., Kulkarni, S. R., Graham, M. J., et al. 2019, *PASP*, 131, 018002 2
- Bianchi, L., Herald, J., Efremova, B., et al. 2011, *Ap&SS*, 335, 161 2
- Blanchard, P. K., Nicholl, M., Berger, E., et al. 2017, *ApJ*, 843, 106 5
- Boroson, T. A., & Green, R. F. 1992, *ApJS*, 80, 109 5
- Cardelli, J. A., Clayton, G. C., & Mathis, J. S. 1989, *ApJ*, 345, 245 7
- Coughlin, E. R., & Nixon, C. J. 2019, *ApJ*, 883, L17 1, 5, 8
- Cutri, R. M., & et al. 2012, *VizieR Online Data Catalog*, II/311 2
- Cutri, R. M., Skrutskie, M. F., van Dyk, S., et al. 2003, *VizieR Online Data Catalog*, II/246 2
- Dai, L., McKinney, J. C., Roth, N., Ramirez-Ruiz, E., & Miller, M. C. 2018, *ApJ*, 859, L20 1
- Donley, J. L., Brandt, W. N., Eracleous, M., & Boller, T. 2002, *AJ*, 124, 1308 1
- Evans, C. R., & Kochanek, C. S. 1989, *ApJ*, 346, L13 1
- Evans, P. A., Beardmore, A. P., Page, K. L., et al. 2007, *A&A*, 469, 379 4
- Evans, P. A., Beardmore, A. P., Page, K. L., et al. 2009, *MNRAS*, 397, 1177 4

- Evans, P. A., Page, K. L., Osborne, J. P., et al. 2020, *ApJS*, 247, 54 4
- Flesch, E. W. 2021, arXiv e-prints, arXiv:2105.12985 2
- Foreman-Mackey, D., Hogg, D. W., Lang, D., & Goodman, J. 2013, *PASP*, 125, 306 5
- Förster, F., Cabrera-Vives, G., Castillo-Navarrete, E., et al. 2021, *AJ*, 161, 242 3
- Gehrels, N., Chincarini, G., Giommi, P., et al. 2004, *ApJ*, 611, 1005 2
- Gezari, S. 2021, *ARA&A*, 59, 21 1, 2, 7, 9, 10
- Guillochon, J., Manukian, H., & Ramirez-Ruiz, E. 2014, *ApJ*, 783, 23 1
- Guo, H., Shen, Y., & Wang, S. 2018, *PyQSOFit: Python code to fit the spectrum of quasars*, *Astrophysics Source Code Library*, record ascl:1809.008 5
- He, Z., Jiang, N., Wang, T., et al. 2021, *ApJ*, 907, L29 5, 6, 9
- HI4PI Collaboration, Ben Bekhti, N., Flöer, L., et al. 2016, *A&A*, 594, A116 4
- Hills, J. G. 1975, *Nature*, 254, 295 1
- Hinkle, J. T. 2022, arXiv e-prints, arXiv:2210.15681 10
- Holoien, T. W. S., Prieto, J. L., Bersier, D., et al. 2014, *MNRAS*, 445, 3263 1
- Jiang, N., Wang, T., Hu, X., et al. 2021, *ApJ*, 911, 31 8, 9, 10
- Johnson, B. D., Leja, J., Conroy, C., & Speagle, J. S. 2021, *ApJS*, 254, 22 2
- Kochanek, C. S. 2016, *MNRAS*, 461, 371 1
- Leja, J., Johnson, B. D., Conroy, C., & van Dokkum, P. 2018, *ApJ*, 854, 62 2
- Lodato, G., & Rossi, E. M. 2011, *MNRAS*, 410, 359 1, 8
- Mockler, B., Guillochon, J., & Ramirez-Ruiz, E. 2019, *ApJ*, 872, 151 1
- Neustadt, J. M. M., Holoien, T. W. S., Kochanek, C. S., et al. 2020, *MNRAS*, 494, 2538 9, 10
- Planck Collaboration, Aghanim, N., Akrami, Y., et al. 2020, *A&A*, 641, A6 2
- Poole, T. S., Breeveld, A. A., Page, M. J., et al. 2008, *MNRAS*, 383, 627 4
- Rees, M. J. 1988, *Nature*, 333, 523 1
- Sánchez-Sáez, P., Reyes, I., Valenzuela, C., et al. 2021, *AJ*, 161, 141 3
- Schlafly, E. F., & Finkbeiner, D. P. 2011, *ApJ*, 737, 103 7
- Strubbe, L. E., & Quataert, E. 2009, *MNRAS*, 400, 2070 1
- Tonry, J. L., Denneau, L., Heinze, A. N., et al. 2018, *PASP*, 130, 064505 3
- Trakhtenbrot, B., Arcavi, I., Ricci, C., et al. 2019, *Nature Astronomy*, 3, 242 10
- Tu, X., & Wang, Z.-X. 2013, *Research in Astronomy and Astrophysics*, 13, 323 2
- van Velzen, S., Pasham, D. R., Komossa, S., Yan, L., & Kara, E. A. 2021a, *Space Sci. Rev.*, 217, 63 8, 9
- van Velzen, S., Gezari, S., Hammerstein, E., et al. 2021b, *ApJ*, 908, 4 1, 2, 4, 5, 8
- Wang, C.-J., Bai, J.-M., Fan, Y.-F., et al. 2019, *Research in Astronomy and Astrophysics*, 19, 149 4
- Wang, T.-G., Zhou, H.-Y., Komossa, S., et al. 2012, *ApJ*, 749, 115 5, 9
- Wang, Y., Jiang, N., Wang, T., et al. 2022, *ApJ*, 930, L4 10
- Wright, E. L., Eisenhardt, P. R. M., Mainzer, A. K., et al. 2010, *AJ*, 140, 1868 2